Left- and right-handed helical tubule intermediates from a pure chiral phospholipid

Britt N. Thomas,[1,2,*] Christopher M. Lindemann,[1] and Noel A. Clark[2,*]
[1]*Department of Chemistry, University of Wyoming, Laramie, Wyoming 82071-3838*
[2]*Condensed Matter Laboratory, Department of Physics, University of Colorado, Boulder, Colorado 80309-0390*
(Received 12 October 1998)

Differential phase contrast microscopy under conditions of very slow cooling reveals the dominant self-assembly mechanism of a chiral diacetylenic phospholipid into multilamellar tubules to be the rapid growth of helical ribbons from spherical multilamellar vesicles. Surprisingly, in the first seconds of tubule formation, a pure enantiomer of 1,2-bis(10,12-tricosadiynoyl)-*sn*-glycero-3-phosphocholine [DC(8,9)PC] yields roughly equal numbers of left- and right-handed helices, inconsistent with the heretofore observed relationship between tubule helix handedness on phospholipid chirality. A much slower process follows by which tubules become multilamellar with a prominent helical ridge upon the exterior. Interestingly, these exterior helical ridges are of only a single handedness. [S1063-651X(99)01203-9]

PACS number(s): 64.70.Md, 61.30.Cz, 61.16.Ch, 64.60.Qb

I. INTRODUCTION

Saturated ethanolic/water solutions of the synthetic diacetylenic phospholipid [DC(8,9)PC] self-assemble upon cooling into hollow cylindrical tube structures, highly unusual for lipids, of typical length $10\,\mu\text{m} < L < 100\,\mu\text{m}$, and diameter $D \approx 0.6\,\mu\text{m}$ [1–3]. A variety of potential applications derive from tubule structural features: they are hollow, may be aligned with magnetic or electric fields [4,5] can be metal plated [6], and are easily polymerized. Electron microscopy shows that the outer layers of multilamellar tubules exhibit a helical structure of handedness related to the molecular chirality [7], strongly suggesting that helically coiled phospholipid bilayer ribbons, such as sketched in Fig. 1(a), are an intermediate structure in tubule formation. Because of its novelty and the apparent role of chirality, the tubule formation process has attracted intense theoretical interest, with descriptions of tubule formation incorporating chirality, originating from either a chiral molecular structure [1,8–14], or from spontaneous achiral symmetry breaking [15].

In this paper we present results of an optical microscopic study of the tubule formation process, observations made possible by providing sample conditions of extremely high-temperature homogeneity and extremely low cooling rate. We confirm that the dominant tubule formation mechanism to be the growth of $L_{\beta'}$ helical ribbons from a high-temperature L_α spherical vesicle phase, driven by an intralamellar L_α-to-$L_{\beta'}$ first-order chain freezing phase transition [16]. Surprisingly, we find that with a pure enantiomer of DC(8,9)PC, the probabilities of forming a left- or right-handed helical ribbons in this initial process are roughly equal, suggesting that the initial helical ribbon formation process is not strongly influenced by intrinsic molecular chirality, i.e., molecular chirality is not the reason that the ribbons are helical, in contrast to all extant interpretations of tubule structure. The rapid lengthwise ribbon growth is concurrent with a slower ribbon broadening leading to closure into a cylindrical tubule. This is followed by a very much slower addition of coaxial outer layers to form a multilamellar tubule. The outer helical windings are uniformly of a single helix sense [right handed for the *R*-DC(8,9)PC enantiomer], indicating that the molecule's chirality is expressed in the slow process of layer addition.

II. EXPERIMENT

A. Tubule preparation

The initial preparation of tubules is standard. The *R* enantiomer of DC(8,9)PC was obtained from the Naval Research Laboratory and synthesized by starting from egg-derived *L*-α-glycerophosphorylcholine [17]. Lipid was dissolved in ethanol/water [75:25 volume to volume (v:v)] at a concentration $c = 1$ mg/ml, by heating with vigorous stirring to $T > T_{L_\alpha \leftrightarrow I}$, the L_α-to-isotropic transition temperature. The so-

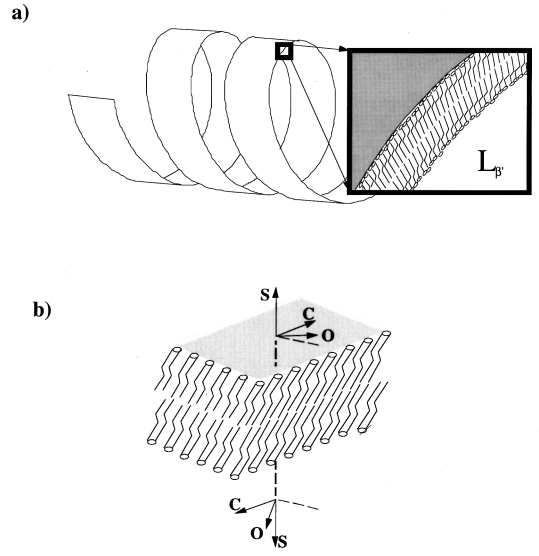

FIG. 1. (a) Schematic diagram of helical tubule intermediate lipid bilayer structure. (b) Schematic diagram of the $\hat{s}$-$\vec{C}$-$\vec{O}$ vector triad characterizing each monolayer and their relative orientation in a bilayer. Monolayer-monolayer interaction involving the oblique ordering $\vec{O}$ will induce bilayer twist.

*Authors to whom correspondence should be addressed.

lution was cooled through $T_{L_\alpha \leftrightarrow L_{\beta'}}$ at approximately 10 °C/h to yield a flocculent precipitate of tubules (typically with $L \approx 20\,\mu$m and a diameter $D \approx 0.6\,\mu$m). This precipitate was centrifuged at 10 000g at 5 °C for 30 min to obtain a concentrated paste, typically with $c = 100$ mg lipid/ml, which was maintained at $T < T_{L_\alpha \leftrightarrow I}$ and diluted to $c = 10$ mg lipid/ml. Optical microscopic examination of the resulting pellet revealed no discernible change in tubule morphology induced by centrifugation.

B. Optical microscopy kinetics probe

The first set of optical microscopy experimental conditions were designed to enable very high-resolution optical microscopic *in situ* real-time observation of the first tubule nucleation and growth events at the L_α (spherical vesicle) to $L_{\beta'}$ (cylindrical tubule) first-order phase transition at $T_{L_\alpha \leftrightarrow L_{\beta'}} = 37$ °C. It was found that concentrations $c \approx 10$ mg lipid/ml were optimal, being large enough to enhance the probability of observing tubule intermediates within the small ($160 \times 100\,\mu$m^2) field of view, but having sufficient separation between vesicles to enable isolated tubule nucleation events. Our previous x-ray diffraction study [16] showed that tubules reversibly cycle between the spherical and cylindrical phases even at these high concentrations, as long as the L_α-to-isotropic transition temperature $T_{L_\alpha \leftrightarrow I} = 57$ °C is never exceeded.

A few drops of the 10-mg lipid/ml solvent preparation were placed in 5-μm-deep optical microscopy cell, gently heated to ≈40 °C to enter the spherical vesicle phase, and examined under cooling. Phase contrast microscopy images were obtained with a Zeiss Axiovert 10 transmission mode microscope with a Zeiss 100× oil-immersion Nomarski differential interference contrast (DIC) objective and condenser, and a Hamamatsu C2400 microscopy video camera coupled to an electronic contrast enhancement module. Great care was exercised to minimize thermal gradients within the cooling sample, and cooling rates less than 0.25 °C/h were necessary in the vicinity of $T_{L_\alpha \leftrightarrow L_{\beta'}}$ (37 °C) to observe tubule formation. The large thermal mass of the microscope, in contact with the heated sample by virtue of its oil-immersion objectives, produced unacceptable thermal gradients within the sample, which were eliminated by placing the entire microscope/video camera assembly in a thermally controlled hutch in which mK sample temperature homogeneity and cooling rates as low as 0.15 °C per hour were reliably attainable. The structure of the evolved tubules was also probed via scanning electron microscopy (SEM) by transferring the sample (lipid solution and tubules) from the optical microscopy cells onto graphite or epoxy substrates, and into the SEM vacuum with no further preparation.

The 5-μm gap between the substrate and the cover slip is larger than the ≈0.6-μm tubule diameter, but far less than the approximately 100-μm length which tubules grow to under very slow cooling [16]. This narrow cell gap forces tubule growth to be primarily parallel to the sample cell plane. However, under our conditions we find the mean tubule diameter to be the same as tubules formed in bulk solutions, and tubule lengths are limited by collisions with other tubules forming in the highly concentrated lipid solution. The narrow gap also flattens larger spherical vesicles in the L_α phase.

C. Optical microscopy tubule interior probe

A Nikon Diaphot 300 inverted microscope equipped with 60× and 100× Nomarski DIC objectives and a Dage VE1000 video camera coupled to a videocassette recorder and high-resolution video capture board was used to image standard-formed tubule interiors. A small amount of the standard 10-mg lipid/ml solvent preparation, known to have uniformly right-handed exteriors, was placed upon a glass microscope slide, air dried, mounted upon the microscope stage, and covered with water. Ethanol was then added to the water incrementally until the outermost layers of the tubule dissolved. Videotapes of the procedure were digitized for analysis.

D. Atomic force microscopy tubule interior probe

Contact-mode atomic force microscopy (AFM) probes of exposed DC(8,9)PC tubule cores were obtained with a Digital Instruments BioScope in the following manner: First, a≈5-mg lipid/ml tubule suspension was drawn across the length of a 24×60-mm glass coverslip and air dried. The dried sample/coverslip assembly was then immersed lengthwise into a 90:10 ethanol:H_2O (v:v) solution over the course of 10 s. This lengthwise immersion generated a solvent-exposure gradient over the length of the coverslip: the first coverslip portion immersed endured approximately $10\frac{1}{2}$ s of solvent exposure, while the last portion was immersed for only about $\frac{1}{2}$ s. The solvent was quickly washed away by placing the coverslip into a large beaker of distilled water and swirling it about. Finally, the sample/coverslip assembly was air dried a second time. This procedure created regions where the uppermost portion of the deposited tubules, that is, the outer lamellae, were dissolved away, exposing the cores, but where the tubules continued to adhere to the glass substrate throughout contact-mode AFM probes.

III. RESULTS

A. Optical microscopy kinetics probe

Figure 2 shows four frames from a video clip of a typical nucleation and growth event, obtained while cooling at 0.25 °C/h. The sequence begins with an L_α spherical vesicle, in which lies a nodule of unknown structure [indicated by the white arrow in (a)] that had appeared several minutes earlier. This nodule initially nucleates three helical ribbons in (b), which are apparently fixed to the nodule and grow in length at a roughly constant velocity of $v \cong 1\,\mu$m/s along the tubule axis. This is followed by many other ribbon nucleations to form a nest of tubules, the growth of which depletes material from the vesicle, as evident in the last frame (d). The reverse process, the slow heating and melting of isolated tubules, occurs by a spherical vesicle forming at one end of the tubule which consumes it with the net volume of the two phases remaining essentially constant, as shown in Fig. 3, suggesting that in this rapid transformation between the spherical and cylindrical phases the principal material transport is between these phases and not to or from the saturated solution. However, we find that slow tubule growth can occur upon

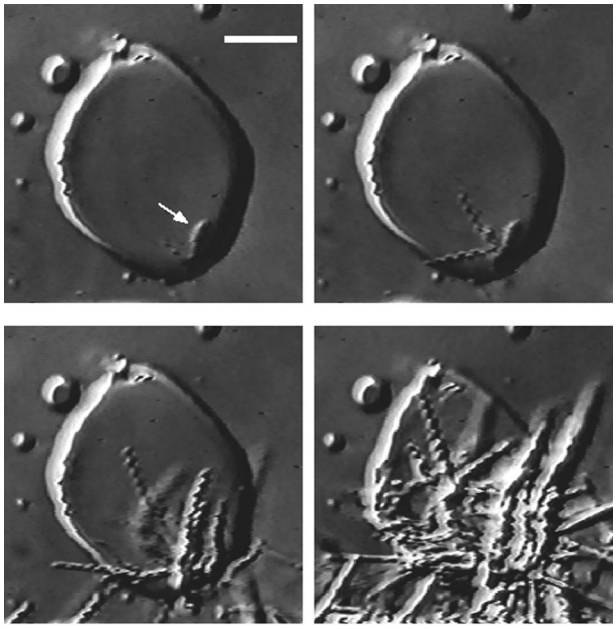

FIG. 2. Four Nomarski DIC microscopy video frames, spaced by 3.1 s and obtained while cooling at 0.25 °C/h, showing DC(8,9)PC $L_{\beta'}$ helical ribbon growth nucleating at a nodule (white arrow) at the edge of a L_{α} spherical vesicle. The nodule appeared 10 min earlier in the cooling cycle. The spherical vesicle is ultimately consumed by the tubules. The scale bar is 5 μm long.

cooling in absence of a spherical vesicle, but that this growth velocity is much slower ($\cong$0.1 μm/s), and, interestingly, nearly the same as that of the addition of outer layers onto already formed tubule cores, as we discuss below.

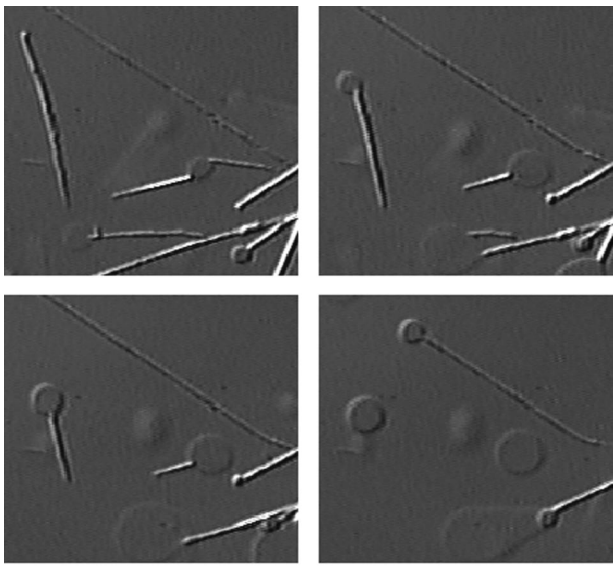

FIG. 3. Four Nomarski DIC microscopy video frames spaced by 3 s obtained while heating at 2 °C/h, showing a DC(8,9)PC $L_{\beta'}$ tubule melting into an L_{α} spherical vesicle. During this process, material is transported principally from the tubule to the vesicle, and not to or from the aqueous solvent. The spherical vesicle almost always forms at a tubule end, as seen in the vertical tubule at the left-hand side of each frame; however, occasionally the spherical vesicle forms along the tubule body, as seen to the right of the vertical tubule in the first frame.

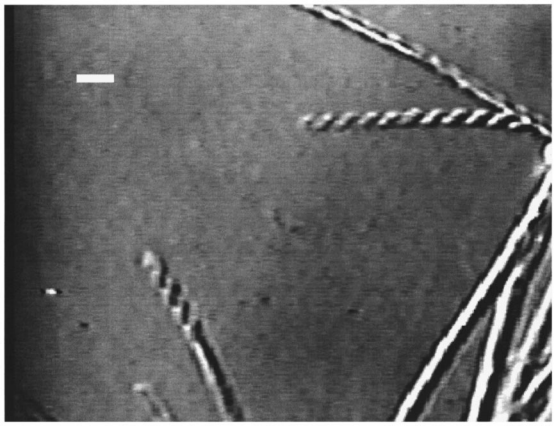

FIG. 4. Nomarski DIC microscopy video frame obtained while cooling at 0.25 °C/h, showing the simultaneous growth of left and right handed DC(8,9)PC $L_{\beta'}$ helical ribbons. The Nomarski images the side of the helix closest to the objective more clearly, preferentially illuminating regions where refractive index increases along the DIC axis. Thus the apparent handedness of the helix winding is not altered by either through focusing or rotation of the sample through any angle. The scale bar is 1 μm long.

A very surprising observation is that both left- and right-handed helices form during a single nucleation/growth event. Figure 4 shows neighboring tubules of opposite handedness having just grown in a vesicle-to-tubule transition of the type depicted in Fig. 2. Occasionally a helix possessing one sense of handedness is seen to sprout from a tubule of the opposite handedness.

These unexpected findings led us to carefully study and consider the role of the DIC microscopic imaging process in determining the apparent helix handedness. *First, we have verified that the apparent helix handedness is independent of the sample orientation, i.e. does not change upon rotation of the sample stage* [18], *and is also independent of the position of the microscope objective focal plane relative to the tubule plane; i.e. apparent helix handedness does not change during a through-focus scan*. In view of the demonstrated invariance of the apparent helix handedness under conditions of varying orientation and focal plane position, images such as Fig. 4 unambiguously show that left and right helices are simultaneously present. Furthermore, the image shows that only one of the helix sides, either the side nearest to objective or furthest from the objective always dominates the helix image.

In transmission microscopic imaging at the high numerical aperture employed here, objects of dimension d in the range $0.5\,\mu\text{m} < d < 1.0\,\mu\text{m}$, or of thicker samples having internal structure in this range, it is the side closest to the objective which is imaged most clearly in a through-focus scan [19]. Thus, in assigning the handedness of a particular tubule, we assume that it is the helix side closest to the objective that is being imaged [20,21].

Additional confirmation of the suitability of DIC optical microscopy, a transmission-mode probe, in helix handedness determination has been provided through atomic force microscopy, a scanning-mode probe [21]. In the aforementioned system, AFM-generated height maps of stable helices allowed unambiguous assignment of helix handedness; left- and right-handed helices were found in the same ratio, as

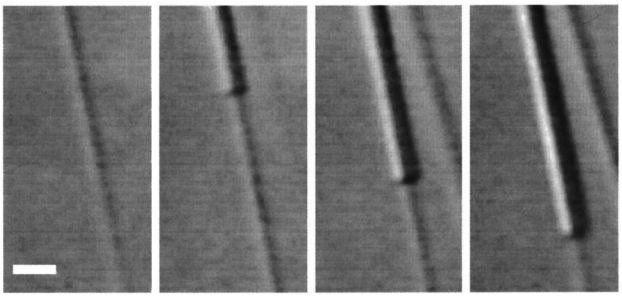

FIG. 5. Four low-magnification Nomarski DIC microscopy video frames spaced by 13 s obtained while cooling at 0.25 °C/h, showing the sheathing of a DC(8,9)PC $L_{\beta'}$ tubule. During this process material is transported to the tubule principally from the cooling saturated solution. The scale bar is 5 μm long.

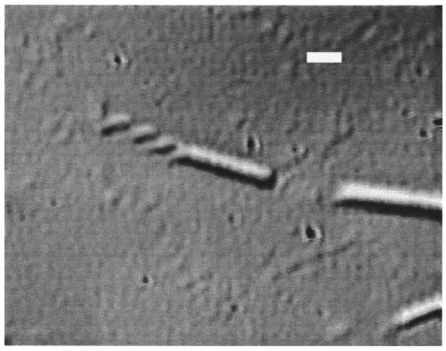

FIG. 6. Nomarski DIC microscopy video image of an exposed DC(8,9)PC tubule core that was formed in bulk solution, and then exposed by dissolution of the tubules' outer layers as described in the text. The scale bar is 1 μm long.

indicated by optical microscopy. While the rapidly-growing helices of the current DC(8,9)PC kinetics study cannot be probed by AFM, we are nevertheless quite confident the optical observation of left- and right-handed cores is correct, and will presently furnish AFM data of exposed DC(8,9)PC tubule cores that further substantiate this point of view.

Efforts to measure the numbers of left- and right-handed helical ribbons in the evolving samples are hindered by the necessarily small field-of-view required for high magnification and the transient nature of the state in which the sense of ribbon handedness was clearly resolvable. (When the helical ribbon has widened to form a closed cylinder, the index of refraction discontinuity found at the ribbon edge/solvent interface, which DIC is optimized to detect, disappears. DIC is, in general, not capable of detecting the helical ridge found on fully formed tubules.) The largest sample from a single event such as in Fig. 2 was ten helices, of which six were right handed and four left handed. Summing identifiable helices from 20 samples yielded a fraction of right-handed helices, $N_R/(N_L+N_R)\approx 0.60$. This surprising result is compounded by the outcome of electron microscopy probes done tens of minutes after such a ''mixed'' sample is observed: all 134 tubules from the sample having $N_R/(N_L+N_R)\approx 0.60$ were found to have right-handed exteriors. This latter observation is in agreement with the previously reported correspondence between molecular chirality and the handedness of the helical ''barber-pole'' stripe found on tubule exteriors [3]. The implication of these observations is *not* that there is a handedness conversion mechanism for the helices, for what we observe with DIC microscopy is the formation of the innermost part of the multilamellar tubules, and what is observed subsequently with SEM is the outermost lamella. Rather, the implication is that there exist tubules with left-handed helices in the core, and right-handed helices on the exterior.

The sequence shown in Fig. 5, a secondary growth about a now-closed helix, several minutes after its formation, suggests a simple mechanism for the apparent change in handedness from the inner to outer lamellae. Our interpretation of the sequence is that the tubule core serves as a nucleation site for phospholipid monomer precipitation from the cooling saturated solution, and so becomes multilamellar. This secondary growth rate is an order of magnitude slower than the initial tubule formation, with approximately 0.1-μm/s axial growth rates as opposed to 1.0 μm/s for the tubule core formation. (Unfortunately, the low magnification required for this sequence does not permit resolution of any underlying helical structure in either lamella.) Occasionally, tubules are seen to form in the absence of spherical vesicles, apparently through the accretion of lipid from the cooling saturated solvent to both ends of the tubule. These ''free-standing'' tubules form concurrently with the secondary growth shown in Fig. 5, and with the same 0.1-μm/s axial growth rate. These similarities suggest that tubule sheathing is also a result of accretion of lipid from solution. Core formation, however, is a very different processes: While ensheathment is the slow accretion of monomer from the cooling, saturated solution, core formation is the rapid conversion of a large reservoir of L_α-phase material (the spherical vesicle), which, due to hysteresis, is usually below $T_{L_\alpha \leftrightarrow L_{\beta'}}$, into $L_{\beta'}$-phase tubule cores. We will argue below that the slower ensheathment process allows molecular chirality to be expressed in the helical sense of handedness, while the rapid L_α-to-$L_{\beta'}$ interconversion does not.

B. Optical microscopy tubule interior probe

Given our particular experimental conditions, namely, the flattening of the larger spherical vesicles by the microscopy cell's size, the anisotropy of the microscopy cells, the high lipid concentrations, and the unusually slow cooling, it was of interest to check whether left-handed cores within right-handed exteriors would appear under the standard tubule formation conditions in bulk solution [7] used initially to prepare the tubules. Tubule interiors were exposed as described in Sec. II B, resulting in structures such as that shown in Fig. 6, in which a left-handed helical core is revealed. Once again, focal-plane translation through exposed tubule cores did not invert the sense of tubule handedness, and the fraction of right-handed tubules was found to be approximately that of the rapidly forming tubule cores in the anisotropic microscopy cells, $N_R/(N_L+N_R)\approx 0.60$.

C. Atomic force microscopy tubule interior probe

The pertinent virtue of AFM is that a true height map of the specimen is created by measuring the vertical deflection of an atomic-dimensioned tip as it is scanned across the specimen. This three-dimensional map enables unequivocal assignment of helix handedness through the unambiguous

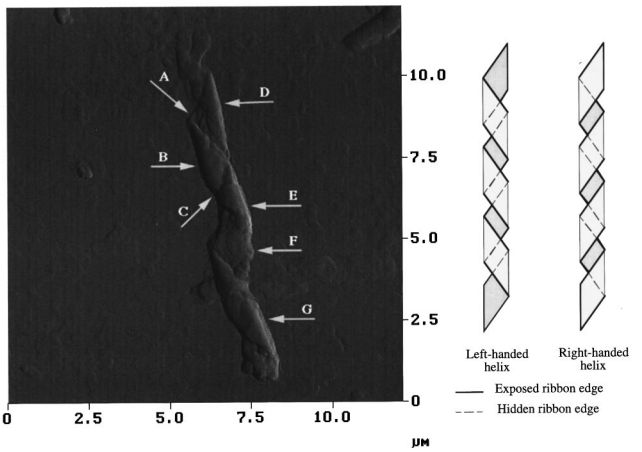

FIG. 7. (left) Contact-mode atomic force micrograph of an exposed DC(8,9)PC tubule core. The handedness of the ribbon is established by distinguishing in the image those parts of the edge of the ribbon which are exposed, i.e., on the top layer, from those parts which are covered by a layer of ribbon. This microstructure possesses a left sense of helical handedness. Note the splotchy residue distributed upon the substrate by tubule dissolution. (right) Schematic drawing of flattened left- and right-handed helical ribbons. The helix exteriors are white, the interiors are gray, and the ribbon edges are drawn to emphasize whether they are exposed to, or hidden from, the observer.

determination of which alternate helix segments are nearer to, or further from, the viewer.

Figure 7 shows a contact-mode atomic force micrograph of a left-handed tubule core exposed through the differential solvation procedure outlined in Sec. II C. The AFM reveals a flattened helical ribbon, composed of areas that lie either $\approx$105 or $\approx$210 nm above the substrate. We interpret the lower-elevation regions (areas *A* and *F*) to be single layers of the flattened helical ribbon and the higher-elevation regions (*D*, *B*, *E*, and *G*) to be double layers. For example, the triangular regions *B* and *E* are nearly coplanar, differing only by the rms surface roughness of 8 nm. (The feature *C* separating regions *B* and *E* is a crease that goes to a depth of 19.0 nm.) The top and bottom portions of the region $\overline{B\,C\,E}$ lie 123.8 and 115.8 nm above regions *A* and *F*, respectively, which in turn lie 102.6 and 103.4 nm below regions *D* and *G*, respectively. The handedness of the ribbon is established by distinguishing in the image those parts of the edge of the ribbon which are exposed, i.e., on the top layer, from those parts which are covered by a layer of ribbon: the ribbon edge in the top layer should image sharply, whereas the covered ribbon edge should not. For example, the crease *C* in high-elevation region $\overline{B\,C\,E}$ corresponds to the expected gap between successive helical ribbon turns on the opposite helix side. The drawing at the left of Fig. 7 illustrates flattened left- and right-handed helices, and the AFM of Fig. 7 is clearly consistent only with a left-handed helical sense.

IV. DISCUSSION

Despite the enantiomerically unambiguous synthesis of our *R*-DC(8,9)PC, and its measured optical rotatory power, which is comparable to the value obtained for pure *R*-DC(8,9)PC quoted by Singh *et al.* [17], indicating that the enantiomeric excess of our sample is near unity, an issue that must be raised at this point is the extent to which any *S*-DC(8,9)PC enantiomer present in the sample would affect the understanding of our results. We examine the ramifications of such chiral contamination by interpreting two of our experimental observations in the context of the Ising-based models of collective achiral symmetry breaking developed by Selinger and Selinger [22] to describe the helical winding of achiral homopolymer chains resulting from the addition of chiral sidegroups [23–26].

First, we observe that all tubule cores are completely left or right handed; that is, there are never kinks in the helices where the sense of handedness changes. In the Ising model of a finite chain (tubule) having N kink sites, this corresponds to a regime where $f = N\exp(-E_k/kT) \ll 1$, f being the number of changes of handedness (kinks) per tubule, and E_k the kink energy. Second, because we observe the nearly racemic 60:40 ratio of left- to right-handed tubules in a system with an enantiomeric excess ($\Phi_{\text{e.e.}}$) near unity ($\Phi_{\text{e.e.}} \cong 1$), we must be in an Ising regime where E_c, the energy difference between an *S* and *R* molecule in, say, a right-handed tubule is quite small. When E_c is small, the collective symmetry-breaking model predicts a nearly linear variation of average helix handedness with enantiomeric excess over the range of $0 < \Phi_{\text{e.e.}} < 1$, with, in particular, nothing dramatic happening as $\Phi_{\text{e.e.}} \to 1$. Thus the Ising model, which works very well to describe the polymer case, indicates that small amounts of chiral impurities, if present, cannot produce the nearly equal numbers of left- and right-handed tubule cores we observe. Furthermore, the Ising model contains precisely the regime we propose for the tubules, namely, large E_k and small E_c.

At the present time there is no satisfactory theoretical model of tubule formation and structure. Our observations provide benchmarks that should serve to guide development of such a model, which must relate the structural feature of DC(8,9)PC required for tubule formation, namely, the phospholipid triple bonds, to the three key aspects of tubule formation: (1) the highly anisotropic $L_{\beta'}$-phase growth velocities in the ribbons, which differ by a factor of $\sim 100\times$ along and perpendicular to the direction of ribbon growth; (2) the curling of the ribbons into helical cores of either handedness; and (3) the uniform handedness of the tubules' outer layers. We now discuss these in turn.

First, our experiments make it clear that the general assumption that the ribbon is an equilibrium structure in the models cited above [8–14] is simply not correct. Clearly, the ribbon is a *growth form*, and not an equilibrium structure. That the ribbon is a growth form is evident since fast growth occurs only as ribbons, whereas slow growth is in the form of sheets or tubes. Indeed, results from our laboratory indicate that the slow-growth bilayers conform to whatever structures are already present, e.g., the helically wound fast-growth ribbons, and thence the entire tubule structure originates in the anisotropy of the fast growth process, and is not an equilibrium structure at all. The growth of ribbons is a form of needle-shaped crystal growth, which occurs, for example, in orthorhombic or hexagonal systems which form low energy surfaces parallel to a high symmetry crystallographic axis.

Second, our experiments call into question the assumption

that the helicity of the ribbons has its origin in molecular chirality. The current theoretical treatments of tubule structure account for the helical curling of the ribbons by combining molecular tilt and intrinsic molecular chirality, since such chirality imparts a tendency for director twist or bend and, as a consequence, a bilayer patch composed of tilted molecules will not be flat but rather saddle shaped in its ground state. Thus, the helical shape of the tubules' $L_{\beta'}$ ribbons has been presumed to arise from such a bilayer twist [8–14]. However, our observations indicate that the helical bilayer twist does not have its origins in molecular chirality, but rather is the result of a spontaneous symmetry breaking to a twisted state, a *twist instability* of an achiral state, similar to that found recently in smectic freely suspended films [27,28], in the ''majority rules'' spontaneous chiralization of achiral homopolymers [23–26], and recently discussed for tilted bilayers of tilted achiral molecules [15]. That is to say, the bilayer has an intrinsic tendency for twist irrespective of handedness, but which is slightly weighted toward right-handed helices by molecular chirality. Thus the bilayer free energy density vs twist is a double-well potential with a barrier ΔF at the planar state (zero twist), and the minimum corresponding to right handed helices which is δF higher than that for left-handed helices, $\delta F \ll \Delta F$, producing a ''majority rules'' instability to one of the helical states. A general observation regarding crystallization is that slowly grown crystals tend to be closer to the thermodynamically ideal structure than rapidly grown crystals. Thus, while molecular chirality favors right-handed ribbons, the fluctuations in the young, rapidly evolving, system permit nucleation of the metastable left-hand state; for the very much slower process of tubule sheathing shown in Fig. 5, the molecule's intrinsic chirality emerges as the determining factor of the outermost layers' uniform right handedness. The result of this process is tubules whose outermost layers are of the expected handedness, but whose inner cylinders may be trapped in the metastable left-handed state.

Our experiments suggest that the carbon-carbon triple bonds in the tails must in some way be responsible for the achiral twist instability. Figure 1(b) illustrates the *minimal* symmetry requirements for a chiral ribbon and a possible mechanism for this effect, in which chirality originates in a way akin to the appearance of chirality of the smectic L phases of achiral molecules [29–32]. For this argument we first consider independently each monolayer of the bilayer, assuming the monolayer to be made of achiral molecules, and characterized locally by $\hat{S}$, the outward-directed monolayer normal, expressing the fact that the outer monolayer surface is different from the interior monolayer surface, and two vector quantities parallel to the bilayer plane: $\vec{C}$ directed along the ribbon growth direction and $\vec{O}$ oblique to $\vec{C}$. Given the highly anisotropic characteristic of ribbon growth it is likely that $\vec{C}$ is parallel to the molecular rows of some Miller index of the hexatic or crystalline lattice. It may also be a molecular tilt direction. There are several vector properties which $\vec{O}$ may represent: (i) the molecular tilt direction if this is a smectic L phase [32]; (ii) the crystallographic direction of the superlattices describing the head group position if there is head group ordering, i.e., if this is an $L_{c'}$ phase [33]; (iii) the glycerol bond joining the two tails in each molecule; and (iv) the direction of oligomerization giving the chain direction if polymerization of the triple bonds into polydiacetylene is initiated. The necessity of the diacetylenic tails suggests that (iv) is the most likely, but (ii) and (iii) cannot be ruled out, since, for example, a preference for a smectic $L_{c'}$-phase may be a consequence of the tail structure.

The $\hat{s}$-$\vec{C}$-$\vec{O}$ triad, and thus any monolayer characterized by such a vector triad, is chiral. For the *bilayer* to be chiral, the handedness of the upper and lower monolayers must be the same, which is obtained by sliding the triad across the top monolayer, around the ribbon edge, and onto the bottom monolayer, with the result shown in Fig. 1(a). Thus, to obtain a chiral bilayer, the handedness chosen in a monolayer symmetry breaking to chirality must propagate to the other monolayer with the same sign. Clearly, the symmetry-allowed interactions between the monolayers involving $\vec{C}$ and $\vec{O}$ will tend to generate a twist of the bilayer. Since we assumed achiral molecules to begin with, the $\hat{s}$-$\vec{C}$-$\vec{O}$ triad of opposite handedness will occur with equal energy.

Our finding of left- and right-handed tubule cores in the *R*-enantiomer also requires the reinterpretation of some extant data. For example, with a model of molecular chirality-driven helix formation, the observation of both left- and right-handed tubules in racemic DC(8,9)PC preparations, could only be interpreted to indicate micro-phase separation of the *R* and *S* enantiomers into left- and right-handed tubules [34]. Our results, indicating that the effect driving the helix formation is not directly related to the molecules' chirality, clearly suggest that helix formation could occur in the racemate without phase separation.

Circular dichroism measurements on DC(8,9)PC solutions show that in the tubule phase there are strongly enhanced molar ellipticities in UV absorption bands [34,35], which can be associated with the diacetylenic group [34]. This data indicate clearly that the molecular chirality results in a much more strongly chiral local environment for the diacetylenic groups in the tubule phase than in the L_{α} phase. On this basis these authors conclude: (i) that the molecular chirality is expressed in some kind of chiral molecular packing in the tubule phase, and (ii) that the chiral packing of the molecules leads directly to the formation of helical ribbons. While the former interpretation is clearly correct, the latter interpretation, which is directly at odds with our observations, is, in fact, not warranted by their data. Specifically, there are in the literature unambiguous counter examples to the assumption that a direct correlation exists between molecular-scale chiral packing and the μm-scale macroscopic expression of chirality. For example, polybenzyl-*L*-glutamate (PBLG) is a homopolypeptide which forms a rod-shaped chirally-packed α-helical structure in a variety of organic solvents, as evidenced by circular dichroism in the UV [36,37]. At sufficiently high concentration these molecules form a chiral nematic phase in which the chirality appears in the form of a micron scale helical winding of the director. However, in achiral binary solvent mixtures of dioxane and methylene chloride, the director helix unwinds with increasing dioxane concentration, with the pitch ultimately diverging to infinity at a particular solvent composition. As more dioxane is added, the helix reforms with the opposite sense of handedness [38]. The UV circular dichroism in these solutions at

lower PBLG concentration (the isotropic phase where there is no contribution to the molar ellipticity from the director helix) remains unchanged through this composition range, indicating that this change in sense of macroscopic helicity occurs with invariant handedness of the molecular α-helical winding [37]. Thus there is no fundamental reason that molecular chirality must result in a particular helix sense or even in a helix at all. While in the PBLG system there is a fixed relationship between helix sense under particular solvent conditions and the chirality of the amino acid side chains, this situation is not found in the tubules. In the tubules there is a strongly collective instability to a state of twist of either handedness which is only weakly biased by chirality. The PBLG data show that macroscopic twist sense can be weakly coupled to molecular packing. Since the model of Selinger and Selinger [22] shows that the limit of weak chiral biasing the ratio of left- to right-handed helices varies linearly with chiral biasing, their model readily accounts for our observation that $N_L/N_R \lesssim 1$.

ACKNOWLEDGMENTS

We gratefully acknowledge the Exxon Research and Engineering Company for their generous extension of office space, microscopy, and computing equipment. We thank R. Shashidar of the U.S. Naval Research Laboratory for providing the phospholipid. B.N.T. and N.A.C. were supported in part by National Science Foundation Grant No. DMR 96-14061 to N.A.C. C.M.L. was supported in part by a grant from the Exxon Education Foundation and by the University of Wyoming Faculty Grant-In-Aid Program. An acknowledgment is made by B.N.T. to the donors of The Petroleum Research Fund, administered by the American Chemical Society, for partial support of this research.

[1] J. M. Schnur, Science **262**, 1669 (1993).
[2] P. Yager and P. E. Schoen, Mol. Cryst. Liq. Cryst. **106**, 371 (1984).
[3] P. Yager, P. E. Schoen, C. Davies, R. Price, and A. Singh, Biophys. J. **48**, 899 (1985).
[4] C. Rosenblatt, P. Yager, and P. E. Schoen, Biophys. J. **52**, 295 (1987).
[5] Z. Li, C. Rosenblatt, P. Yager, and P. E. Schoen, Biophys. J. **54**, 289 (1988).
[6] J. M. Schnur, P. E. Schoen, P. Yager, J. M. Calvert, J. H. Georger, and R. Price, US Patent No. 4,911,981 (March 1990).
[7] J. H. Georger, A. Singh, R. R. Price, J. M. Schnur, P. Yager, and P. E. Schoen, J. Am. Chem. Soc. **109**, 6169 (1987).
[8] P. G. de Gennes, C. R. Acad. Sci. Paris **304,** 259 (1987).
[9] W. Helfrich and J. Prost, Phys. Rev. A **38**, 3065 (1988).
[10] W. Helfrich, J. Chem. Phys. **85**, 1085 (1986).
[11] T. C. Lubensky and J. Prost, J. Phys. II **2**, 371 (1992).
[12] Z. Ou-Yang and J. Liu, Phys. Rev. Lett. **65**, 1679 (1990).
[13] J. V. Selinger and J. M. Schnur, Phys. Rev. Lett. **71**, 4091 (1993).
[14] J. V. Selinger, F. C. MacKintosh, and J. M. Schnur, Phys. Rev. E **53**, 3804 (1996).
[15] U. Seifert, J. Shillcock, and P. Nelson, Phys. Rev. Lett. **77**, 5237 (1996).
[16] B. N. Thomas, C. R. Safinya, R. J. Plano, and N. A. Clark, Science **267**, 1635 (1995).
[17] A. Singh, T. G. Burke, J. M. Calvert, J. H. Georger, B. Herendeen, R. R. Price, P. E. Schoen, and P. Yager, Chem. Phys. Lipids **47**, 135 (1988).
[18] DIC microscopy utilizes variations in the specimen refractive index by combining two slightly displaced images along the so-called DIC optical translation axis. This displacement brightens regions where the refractive index increases along the DIC optical axis, and *vice versa*. The potential for dependence of perceived helix handedness upon orientation with respect to the DIC axis was investigated by rotating isolated helices through 180° with respect to the DIC axis. It was found that the apparent helix handedness does not change upon reorientation of the helix about the DIC axis. However, as one should expect, the image quality of the helix does depend upon the orientation of its ribbon edges relative to the shadowing DIC axis.
[19] T. Wilson, *Confocal Microscopy* (Academic, London, 1990).
[20] Note that even if this assumption were not correct, the basic conclusion of the paper, namely, that roughly equal numbers of left- and right-handed tubules are present early in the growth process, would not be affected.
[21] B. N. Thomas, R. C. Corcoran, C. L. Cotant, C. M. Lindemann, J. E. Kirsch, and P. J. Persichini, J. Am. Chem. Soc. **120**, 12178 (1998). Concerns about the imaging characteristics of μm-dimensioned helical structures led us to carry out a variety of imaging experiments on tubules made of a DC(8,9)PC phosphonate analog of diameters D in the range $1.0\ \mu\text{m} < D < 3\ \mu\text{m}$. In solution those tubules are cylindrical, but AFM shows they flatten to a 50-nm height (about four bilayers) upon deposition and desiccation on a glass substrate. The imaging process may be thought of most simply as the intersection of the focal plane, having a certain depth of focus δ with the helix. The perceived helix image will in general depend upon the location of the plane of focus relative to the helix axis, i.e., whether it is closer to or further from the objective, and on the relative magnitudes of δ and D. The flattened helical ribbons lie entirely within the depth of focus of the objective (i.e., $\delta \gg 40\ \text{nm}$), and both sides of the helix (nearest to and furthest from the objective) are simultaneously in focus and of equal clarity (cf. Fig. 9 of this reference). In this case it is impossible to determine helix handedness. On the other hand, the sides nearest to and furthest from the objective in unflattened helical ribbons with $D \approx 3\ \mu\text{m}$ are separated by a distance larger than δ, and therefore can be imaged independently. In this case the helix handedness apparently reverses during a focus scan through the helix, as intersection of the focal plane with the opposite helix sides should produces images that indicate opposite senses of handedness, i.e., reflected through and shifted along the helix axis by $\frac{1}{2}$ pitch (cf. Fig. 9 of this reference). However, when D is 1 μm, it is found that the image of the helix side further from the objective becomes unresolvable and only the helix side nearest the objective can

be imaged. This is also the situation for ≈0.6-μm-diameter DC(8,9)PC helical structures of this study.

[22] J. V. Selinger and R. L. B. Selinger, Mol. Cryst. Liq. Cryst. Sci. Technol., Sect. A **288**, 33 (1996).

[23] M. M. Green, T. Sato, A. Teramoto, and S. Lifson, Macromol. Symp. **101**, 363 (1996).

[24] M. M. Green, N. C. Peterson, T. Sato, A. Teramoto, R. Cook, and S. Lifson, Science **268**, 1860 (1995).

[25] C. A. Khatri, M. M. Green, and H. Morawetz, Polym. Prepr. (Am. Chem. Soc. Div. Polym. Chem.) **35**, 807 (1994).

[26] M. M. Green, C. Khatri, and N. C. Peterson, J. Am. Chem. Soc. **115**, 4941 (1993).

[27] J. Pang and N. A. Clark, Phys. Rev. Lett. **73**, 2332 (1994).

[28] M. Seul and J. Maclennan, Phys. Rev. Lett. **69**, 2082 (1992).

[29] G. S. Smith, C. R. Safinya, D. Roux, and N. A. Clark, Mol. Cryst. Liq. Cryst. **144**, 235–55 (1987).

[30] G. S. Smith, E. B. Sirota, C. R. Safinya, R. J. Plano, and N. A. Clark, J. Chem. Phys. **92**, 4519 (1990).

[31] E. B. Sirota, G. S. Smith, C. R. Safinya, R. J. Plano, and N. A. Clark, Science **242**, 1406 (1988).

[32] G. S. Smith, E. B. Sirota, C. R. Safinya, and N. A. Clark, Phys. Rev. Lett. **60**, 813 (1988).

[33] V. A. Raghunathan and J. Katsaras, Phys. Rev. Lett. **74**, 4456 (1995).

[34] J. M. Schnur, B. R. Ratna, J. V. Selinger, A. Singh, G. Jyothi, and K. R. K. Easwaran, Science **264**, 945 (1994).

[35] M. S. Spector, J. V. Selinger, and J. M. Schnur, J. Am. Chem. Soc. **119**, 8533 (1997).

[36] I. Tinoco, R. W. Woody, and K. Yamaoka, in *Rotatory Dispersion: Related Theory and Applications, 1960*, edited by B. D. Levedahl and T. W. James (Pergamon, Oxford, 1961), Tetrahedron **13**, 134 (1961).

[37] J. T. Yang, in *Rotatory Dispersion: Related Theory and Applications, 1960* (Ref. [36]); Tetrahedron **13**, 143 (1961).

[38] C. Robinson, in *Rotatory Dispersion: Related Theory and Applications, 1960* (Ref. [36]); Tetrahedron **13**, 219 (1961).